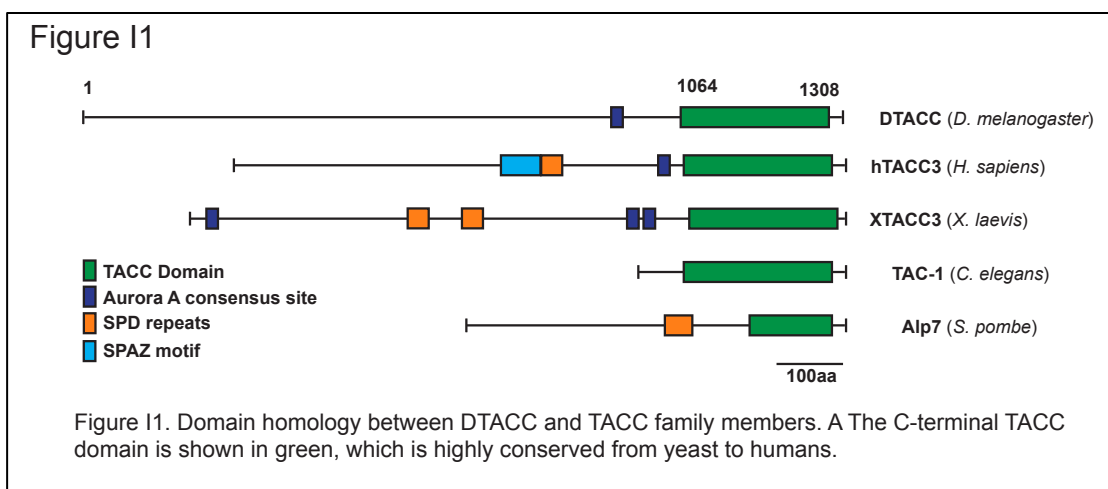


**Abstract**

Microtubules (MTs) are essential for numerous cellular processes. MTs impact cell shape, serve as intra-cellular transport tracks, and form the mitotic spindle. Microtubule-associated proteins (MAPs) modulate MTs to afford differing MT dynamics and ultra-structure. The TACC proteins, a highly conserved MAP family, localize to the MT plus-end and to centrosomes where they affect MT dynamics and interact with other MAPs to modulate their MT-regulating potency. We focus on the interplay between TACC and the MT polymerase, XMAP215. To elucidate TACC's mechanisms of centrosome-localization and XMAP215-recruitment in cells, we used *Drosophila* S2 cells as a model cell system. We used truncational analysis of *Drosophila* TACC (DTACC) in order to identify regions of DTACC that localize to the centrosome and to MT plus-ends using fluorescence microscopy. These results suggest the determinants of DTACC that confer *in vivo* Msp ( *Drosophila* XMAP215) binding and are consistent with our *in vitro* biochemical binding assays.

## Introduction

The cytoskeleton provides structural support and allows for cellular motility, intracellular transport, and chromosomal segregation in eukaryotic cells. The three main components of the cytoskeleton are actin filaments, intermediate filaments, and microtubules (MTs). This study focuses on MTs, which establish cell polarity for directed migration, create pathways for intracellular transport, and form the bipolar spindle during cell division. During interphase, MTs make up the vast network responsible for cellular structure and intracellular transport. At the onset of mitosis, however, the MT network is restructured to form the characteristic bipolar spindle necessary for chromosome separation and cell division. The bipolar spindle is a three-dimensional oval structure formed by MTs radiating from two centrosomes at opposite ends of the cell (as discussed in Tuszynski *et al.*, 1997). Centrosomes are composed of a nine-fold symmetric centriole surrounded by a coat of proteins known as the pericentriolar material (PCM). PCM proteins nucleate and regulate MT dynamics; however, the mechanisms by which these events are regulated remain poorly understood (as discussed in Glover, *et al.*, 1993). One protein family in particular, the TACC (transforming acidic coiled coil) family, has been shown to localize to centrosomes where it has been shown to affect MT density. Thus, it has been



hypothesized to play a role in MT nucleation and/or stability at the centrosome. Despite the discovery of the TACC family over fifteen years ago, there is little structural or mechanistic information on how the TACC family interacts with or regulates MTs.

The TACC protein family is conserved across a wide variety of eukaryotic organisms including *C. elegans*, *D. melanogaster*, *X. laevis*, and *H. sapiens* (as discussed in Peset and Vernos, 2008) (Figure I1). In humans, there are three TACC homologues: TACC1, TACC2, and TACC3. Human TACC3 was first observed via its over-expression in malignant tumors (Still *et al.*, 1999). Every TACC homolog shares a highly conserved 200-amino acid domain at its C-terminus, which is predicted to form a coiled-coil. This coiled-coil domain has been shown to confer localization to the centrosome and is thought to contribute to the stability of the spindle (Gergely *et al.*, 2000). Furthermore, the coiled-coil domain of TACC family of proteins has been shown to interact with the C-terminal region of the XMAP215 family (*Xenopus* microtubule-associated protein, 215 kDa). The XMAP215 family is a well-studied MT plus-end localizing protein family that increases both the polymerization and depolymerization rates of MTs (Shirasu-Hiza *et al.*, 2003). Just as the TACC and XMAP215 families are conserved across evolution, so too is the TACC-XMAP215 interaction. XTACC3 and XMAP215 function together in *X. laevis* to attach MTs to the centrosome (Albee and Wiese, 2008). In *C. elegans*, TAC-1 (TACC family) and ZYG-9 (XMAP215 family) function together to promote MT polymerization and stabilize each other (Bellanger and Gönczy, 2003). In humans, TACC3 and ch-TOG (XMAP215 family), along with other protein factors, form complexes that stabilize kinetochore MTs during mitosis (Booth *et al.*, 2011).

Just as the cooperation of the XMAP215 and TACC families to regulate MTs is conserved, so too are the physical interactions between the two families are of interest. Despite

the conserved interaction of large regions of each protein, current literature suggests that the specific TACC and XMAP215 residues that afford this interaction differ greatly between species (Hood *et al.*, 2013; Thakur *et al.*, 2014; Mortuza *et al.*, 2014). This lack of “agreement” of the TACC-XMAP215 interacting regions remains one of the most poorly understood aspects of the TACC family. Thus, I set out to resolve this discrepancy in the field. To further understand the interaction of these two proteins, I chose to work with the *Drosophila* homologue of the TACC family (DTACC), as the specific residues of DTACC that interact with the *Drosophila* XMAP215 homologue, Minispindles (Msps), have not been elucidated.

DTACC is known to localize to the centrosome during mitosis (Gergely *et al.*, 2000), and our lab has observed DTACC localization to MT plus-ends when expressed *in vivo* (Figure S1). DTACC is necessary for proper *Drosophila* embryonic development, as DTACC mutant embryos exhibit abnormal spindles, shorter MTs, and chromosome missegregation (Raff *et al.*, 2002). Mutant DTACC cellular phenotypes suggest that DTACC stabilizes the bipolar spindle at the centrosome, although the mechanism for this stabilization remains unknown.

In order to resolve discrepancies in the field of how the TACC family interacts with the XMAP215 family and how this interaction in turn regulates MTs, I sought to understand the specifics of how DTACC binds Msps.

Since the evolutionarily conserved TACC domain sequence interacts with Msps *in vivo*, it follows that the TACC domain should have a conserved structural motif that affords its Msps-interaction function. Despite the lack of any definitive DTACC tertiary structure, secondary structure software predicts the TACC domain forms a coiled-coil. Previous research in the Slep lab using truncational analysis of DTACC’s coiled-coil domain identified a minimal region of the TACC domain (residues 1177-1308) that localizes to both centrosomes and to MT plus-ends

when expressed in cell culture (Figure S2). This localization was shown to be Msps-dependent (Figure S1). In order to elucidate the specific residues involved in the DTACC-Msps interaction, I designed a set of experiments that mutated specific residues in this DTACC region, and I then assayed for the ability of the mutant proteins to interact with Msps.

Secondary structure predictions suggest that the TACC domain forms a coiled-coil, which is a highly  $\alpha$ -helical superstructure. Hydrophobic residues on the inner surfaces of these  $\alpha$ -helices typically mediate coiled-coil formation, while hydrophilic residues on the solvent-exposed helical surfaces can confer binding to other cellular factors. Using secondary structure prediction software and sequence-homology alignments between DTACC and its homologues, I identified a set of highly conserved, charged residues throughout the TACC domain (Figure S3). I hypothesize that these charged residues create a charge-specific binding surface on the TACC domain coiled-coil, which mediates the DTACC-Msps interaction. To test these hypotheses, I have used a combination of cell biological, biochemical, and structural techniques that have further characterized DTACC's structure and its interaction with Msps. The results of these experiments have enabled me to determine specific residues and regions on DTACC that confer localization to MT plus-ends and to centrosomes. Thus, I have added to the field an additional set of TACC/XMAP215 data to further characterize the interaction between these two families.

## **Materials and Methods**

### **A. Cloning and Expression**

I amplified *dtacc* fragments (residues 1064-1304, 1092-1304, 1119-1304, 1135-1304, 1158-1304, 1177-1304) using PCR, restriction digested the PCR fragments, and ligated each fragment separately into pET-28 b, a bacterial expression vector with a PreScission protease-

cleavable poly-histidine (poly-his) tag. In addition to pET-28 b, I also ligated *dtacc* 1064-1304 cDNA into pENTR/D-TOPO (Life Technologies), an *E. coli* entry vector and then transferred the insertion to pDEST 15, a bacterial destination vector with a glutathione *S*-transferase (GST) tag. I amplified and purified each construct using XL1B *E. coli* cells and a standard Miniprep protocol before confirming the correct insertion of each *dtacc* cDNA using sequence analysis.

I transformed DTACC plasmids into BL21 DE3 (pLysS) *E. coli* cells and grew the cells in 6 L of selective lysogeny broth (LB) at 37 °C until the cells reached an optical density of 0.600-0.800 at a wavelength of 600.0 nm. I induced the cells with 10 mM Isopropyl  $\beta$ -D-1-thiogalactopyranoside (IPTG) and shook for 24 hours at 18 °C before harvesting the cells. I centrifuged the cells at 3,500 rpm for 10 minutes at 4 °C and resuspended the bacterial pellet in 150 mL of Ni<sup>2+</sup>-NTA Buffer A (25 mM Tris pH 8.0, 300 mM NaCl, 10 mM Imidazole, 0.1% 2-Mercaptoethanol). I resuspended the GST bacterial pellet in GST Buffer A (25 mM Tris pH 8.0, 300 mM NaCl, 0.1% 2-Mercaptoethanol ( $\beta$ ME)). I treated the resuspended pellet with 1.0 mM PMSF protease inhibitor and lysed each growth of cells using three cycles of sonication. I centrifuged the lysate at 15,000 rpm at 4 °C for 45 minutes before extracting the supernatant. To test for expression and solubility of the novel DTACC protein constructs, I took 1.0-mL samples of each DTACC bacterial growth at each of the four steps in the DTACC expression process: pre-IPTG-induction, post-IPTG-induction, post-centrifugation pellet (insoluble fraction), and post-centrifugation supernatant (soluble fraction). I separated the samples using sodium dodecyl sulfate polyacrylamide gel electrophoresis (SDS-PAGE) at 200 V for 40 minutes to confirm expression and solubility of each of the DTACC constructs.

## B. Protein Purification

For the expressed DTACC-poly-his constructs, I loaded the centrifugation supernatant for each poly-his-tagged construct onto separate Ni<sup>2+</sup>-NTA columns (Qiagen). I washed off unbound sample with 250 mL Ni<sup>2+</sup>-NTA Buffer A, and eluted the proteins with a fractionated, linear imidazole gradient (10-150 mM). I identified protein-containing fractions with SDS-PAGE before cleaving the poly-his tag from the fractionated proteins using a PreScission protease. I dialyzed out excess imidazole and poly-his into 3 L of Ni<sup>2+</sup>-NTA Buffer A for 18 hours at 4 °C. I passed each cleaved DTACC construct through another Ni<sup>2+</sup>-NTA column to separate the cleaved proteins from uncleaved protein, remaining poly-his, and PreScission protease. I concentrated the Ni<sup>2+</sup>-NTA-purified DTACC constructs with multiple 20-minute centrifugation steps at 4,000 rpm in an appropriate size-exclusion column (10-30 kDa). I transferred and concentrated each DTACC construct into protein storage buffer (130 mM NaCl, 10 mM HEPES pH 8.0) to concentrations of 5-10 mg/mL.

For the purification of DTACC 1064-1304-GST, I mixed the centrifugation supernatant with GST-coated beads in GST Buffer A, and incubated the bead slurry on a rotator for 18 hours at 4 °C to allow sufficient binding. I loaded the bead slurry into a flow column and washed the beads with 600 mL GST Buffer A. I batch eluted the DTACC-GST with 50 mL of fresh GST Buffer B (25 mM Tris pH 8.0, 25 mM reduced glutathione, 300 mM NaCl, 0.1% βME). I concentrated DTACC-GST to 5 mg/mL in protein storage buffer. For control pull-down experiments involving DTACC-GST, I also expressed and purified GST alone (according to the same protocols above) and concentrated GST to 80 mg/mL.

### C. Circular Dichroism

I performed circular dichroism (CD) with the assistance of Rebecca Adikes, Amy Howard, and Dr. Ashutosh Tripathy (UNC-CH MAC-IN-FAC) using a Chirascan Plus Steady State CD spectrophotometer. I diluted the protein concentration to 0.1-0.5 mg/mL for the CD scan and temperature ramps. We took background scans at 20 °C with and without CD buffer (10 mM NaPO<sub>4</sub> pH 7.5, 30 mM NaF) from wavelengths of 185-260 nm with a step size of 0.5 nm, a 1-nm bandwidth, and 1.25 s per point. We took sample scans with the same parameters. For each sample, we took CD over a 20-94 °C temperature ramp at 208 and 222 nm wavelengths. The protein samples on which we performed CD were DTACC 1177-1304 and 1064-1176 (both purified beforehand by Rebecca Adikes).

### D. GST Pull Down Assays

I resuspended Glutathione magnetic beads (Pierce) and aliquoted 50 µL of the bead slurry (12.5 µL of pure beads) into separate microcentrifuge tubes. I magnetically separated the beads from the supernatant before removing the supernatant. I washed the beads with three rounds of 300 µL GST bead wash buffer (125 mM Tris pH 8.0, 150 mM NaCl, 0.1% βME). I resuspended the beads and added purified DTACC 1064-1304-GST fusion protein to a final concentration of 10 ng of protein per 1 µL of beads to a final total volume of 300 µL. I incubated the beads on a nutator for 18 hours at 4 °C before washing three times. I saved each supernatant sample before boiling them with SDS-PAGE loading dye. I added Msps C-terminal fragments (purified by Rebecca Adikes) to the resuspended bead slurry for a final DTACC:Msps molar ratio of 1:1 and a final volume of 300 µL. I incubated and washed the beads according the same protocol above. I then boiled the beads with 100 µL of 1X SDS-PAGE loading dye before analyzing the supernatant and eluate samples with SDS-PAGE.

### E. Protein Crystallization

I performed all crystallization assays using the hanging-drop method at 4 °C. The trays, well solutions, and glass cover slides were pre-cooled to 4 °C before introducing protein. I thawed DTACC 1064-1304 at ~5 mg/mL on ice (0 °C) and further concentrated to ~10 mg/mL using multiple 20-minute centrifugation steps at 4 °C. I then performed an aggregate-clearing spin at 50,000 rpm at 4 °C for 10 minutes. I immediately used the cleared protein to make crystal drops with a v/v ratio of 1:1, 2:2, or 1:3 protein to crystallization solution. I made control drops using the same ratio of protein storage buffer and crystallization solution. Trays were incubated for at least 24 hours at 4 °C before observations of ~10 minutes at 23 °C. The broad-screen well solutions used were HR2-126 PEG-Ion Screen or HR2-110 Crystal Screen (Hampton Research). All other solutions used the following ranges of conditions: 10-40% 2-propanol, 0.1-0.2 M sodium cacodylate pH 5.0-7.0, and 0.10-0.30 M sodium citrate.

### F. Mutation Design and Cloning

I selected 14 evolutionarily conserved, charged residues in DTACC 1177-1308 using sequence alignments and secondary structure predictions. To test the importance of the 14 charged TACC domain residues in Msps binding, I designed missense mutations to these residues that either ablated or reversed the conserved charge. I generated 14 mutant constructs within DTACC 1177-1308 using QuikChange (QC) reactions with primers containing the desired mutations. The 14 mutations cloned were as follows: E1186K, E1197K, N1223E, R1230E, Y1231A, Y1231F, K1235A, K1235E, H1237E, Q1241E, N1246E, E1259K, QK1283-4AE, E1296K. For further analysis, I also selected and cloned seven of these mutations into *dtacc* 1064-1308, which were as follows: R1230E, Y1231F, K1235E, K1235A, N1246E, QK1283/4AE, E1296K. I performed QC reactions on wild-type DTACC in a pIZ-pMT vector

that contains a metallothionein promoter and a C-terminal green-fluorescent protein (GFP) tag. After QC, I treated the DNA with Dpn1 for one hour and transformed into XL1B *E. coli* cells using a standard transformation protocol. I amplified and purified the plasmids using a standard Miniprep protocol.

#### G. Cell Culture/Imaging

For the DTACC mutations, I treated *Drosophila* S2 cells daily with 2  $\mu$ L of RNA that targets the N-terminus of DTACC for a total of seven days. I co-transfected the cells with 1000 ng of mutant DTACC-GFP DNA and 1000 ng of  $\alpha$ -tubulin-mCherry DNA (provided by Dr. Steve Rogers lab) using an Amaxa S2 electroporation transfection protocol 48 hours before imaging. I induced protein expression with 0.5  $\mu$ L of 100mM CuSO<sub>4</sub> 24 hours before imaging. I plated the induced cells onto Concanavalin A (ConA)-coated glass bottom petri dishes and incubated for 30 minutes at 23 °C. With the assistance of Dr. Jaime Fox, I collected time-lapse images of the co-transfected S2 cells with a 100x NA 1.45 Plan Apochromat objective using a VT-Hawk (VisiTech) software system with an Orca-R2 CCD camera controlled using VisiTech Vox software.

For the mitochondrial KnockSideways (KS) experiments, I obtained a pre-cloned PAtrFPTom20DTACC construct (Rebecca Adikes) containing a mitochondrial localization (mito) sequence, a red fluorescent protein tag (trFP), and *dtacc* 1064-1308. I co-transfected S2 cells with 750 ng of PAtrFPTom20DTACC and 750 ng of Msps 1596-2042-GFP DNA. I induced the cells according to the same protocol as above and imaged the cells using Nikon widefield epifluorescence microscope (100x objective).

## Results

### A. Structure of DTACC C-terminal Region is $\alpha$ -helical and Dimeric

We hypothesize that DTACC interacts with Msps through its C-terminal coiled-coil domain, so we first probed the C-terminal domain using CD to determine if this domain was alpha helical. CD of three DTACC truncations (1177-1304, 1064-1176, and 1064-1304) were taken to characterize the secondary structure of different regions of the C-terminal TACC domain. Wavelength CD of both DTACC 1177-1304 and 1064-1177 (Figure 1A,C) showed absorbance minima at 208 and 222 nm. Temperature ramp CD at 208 and 222 nm for each construct (Figure 1B,D respectively) showed a low melting curve for each fragment; a melting temperature ( $T_m$ ) could not be calculated for either fragment. The full TACC domain (1064-1304) had similar CD minima at 208 and 222 nm wavelengths (Figure 1E), and the temperature ramp CD revealed a characteristic melting curve with a  $T_m$  of 32 °C.

Because coiled-coils typically mediate dimerization, we tested populations of purified DTACC C-terminal fragments for oligomerization using SEC-MALS. Dynamic light scattering revealed that DTACC 1064-1304 (Figure S4A) primarily exists as population of dimers with an observed molecular weight (MW) of 59.4 kDa. Similarly, DTACC 1177-1304 (Figure S4C) also presented as a dimer with a MW of 28.8 kDa. DTACC 1064-1176 (Figure S4B) was the only truncation analyzed that consisted of a monomer population with a MW of 14.5 kDa. Thus, we confirmed that the TACC domain dimerizes, and we identified which TACC domain fragment is necessary for dimerization.

Figure 1

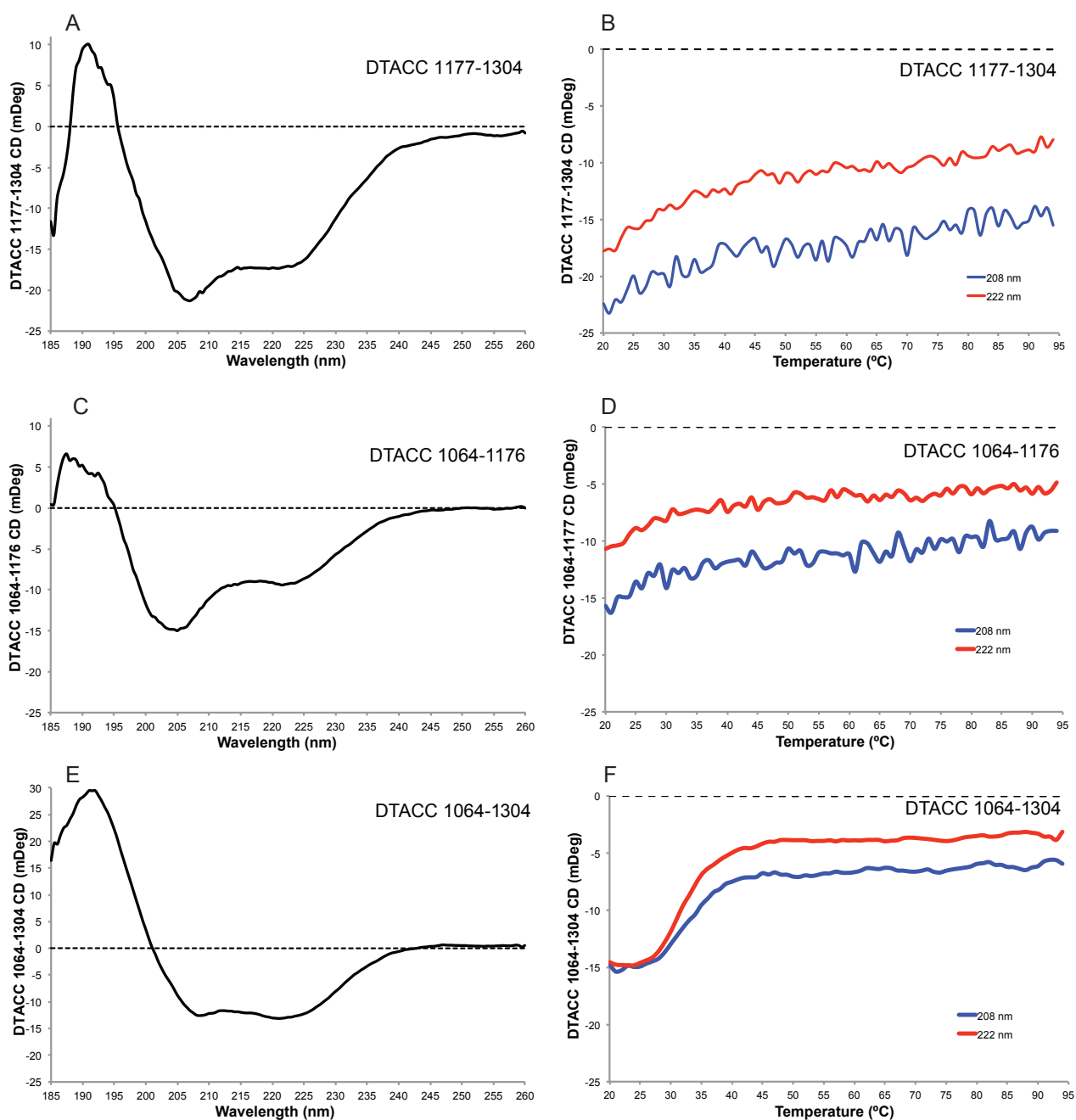


Figure 1. CD of DTACC C-terminal region. The DTACC constructs used for CD were: 1177-1304 (A,B), 1064-1176 (C,D), and 1064-1304 (E,F; performed by Rebecca Adikes). CD were taken at wavelengths of 185-260 nm (first column), and then at 208 nm and 222 nm from a temperature range of 20 °C to 94 °C (second column). All three fragments of the TACC domain show alpha helical character with CD absorbance minima at 208 nm and 222 nm (A, C, E). DTACC 1064-1304 is the most thermostable fragment (F) in comparison to its two subfragments (B,D), as signified by the more robust melting curve. The  $T_m$  of 1064-1304 was calculated to be 32 °C.

To directly characterize the TACC domain structure and confirm its coiled-coil structure via X-ray protein crystallography, I attempted to crystallize purified DTACC. To first determine which conditions favor DTACC crystal formation, 96 different Hampton Research solutions were used to broad screen for potential crystals of Ni<sup>2+</sup>-NTA-purified DTACC 1064-1304 at a concentration of 10 mg/mL. The only solution to yield reproducible results was HR2-110 #8 (0.2 M sodium citrate tribasic dehydrate, 0.1 M sodium cacodylate trihydrate pH 6.5, 30% v/v 2-propanol). The initial crystals in this broad-screen condition are visible under polarized light in Figure 2A. Optimization trays were set up around HR2-110 #8 that varied the concentrations of the salt (sodium citrate), buffer (sodium cacodylate), and precipitate (isopropanol), as well as the pH of the solution. Most preliminary crystallization occurred at 20% isopropanol, 0.2 M sodium citrate, and pH values between 5.0-5.5. Crystals formed most often in drops with a protein volume to well solution volume ratio of 2:2  $\mu$ L, and with an initial protein concentration of  $\sim$ 10 mg/mL. These optimization conditions also had no salt crystals form in control drops. An example of a potential optimized DTACC 1064-1304 crystal can be seen in Figure 2B.

Figure 2

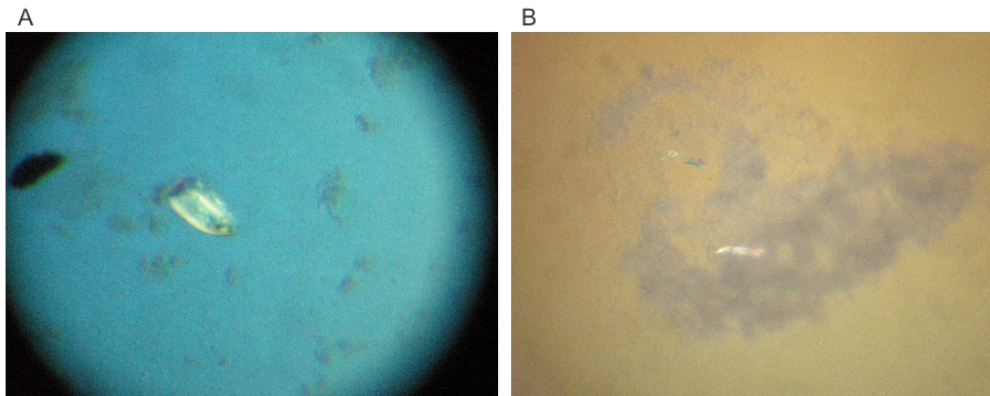


Figure 2: Potential DTACC 1064-1304 (10 mg/mL) crystals. Crystal A formed in Hampton Research Broad Crystal Screen 110, Condition #8 (0.2 M Na Citrate, 0.1 M Na Cacodylate pH 6.5, 30% 2-Propanol) at 4 °C. Crystal B formed in an optimization solution (0.1 M Na Cacodylate pH 5.0, 0.2 M NaCitrate, 20% isopropanol) at 4 °C. Both images are shown though a polarizing filter.

## B. DTACC Mutational Analysis Reveals Msps- and Centrosome-localization Regions

We hypothesized that certain charged residues within the second half of the TACC domain (residues 1177-1308) constitute a charge-specific binding surface for Msps. To test this hypothesis, I cloned the 14 DTACC mutation constructs into DTACC 1177-1308 and expressed in *Drosophila* S2 cells. These S2 cells were depleted of endogenous DTACC via RNAi at the time of expression of exogenous DTACC mutants. To visualize the mutant DTACC constructs' abilities to localize to MT plus-ends (and thus interact with Msps), I performed fluorescence microscopy of each mutant DTACC construct-transfected S2 cells. The resulting time-lapse images of single cells were scored on the ability of its mutant DTACC construct to localize to MT plus-ends, the MT lattice, and, if the cell was mitotic, to centrosomes. Each of the 14 DTACC 1177-1308 mutations and a representative interphase image are shown in Figure 3. Those images with white box insets represent noticeable DTACC localization to MT plus-ends during interphase. A quantification of the mutant DTACC 1177-1308 constructs' abilities to localize to MTs during interphase is provided in Table 4A. A bar graph of the data presented in Table 4A can be seen in Figure 4B that illustrates the decreased MT localization observed in certain DTACC mutations, in comparison to the WT DTACC 1177-1308 localization patterns. These data were used to determine which DTACC charged residues were important for Msps binding.

We selected six of the mutations introduced to DTACC 1177-1308 for further analysis in a different DTACC construct (marked with \* in Figure 4B). These mutations were selected with a focus on deleterious mutations that ablated DTACC's ability to localize to MT plus-ends, as well as similar charge reversal mutations that were not deleterious. The six mutations were cloned into the full TACC domain (1064-1308), transfected into S2 cells, and imaged

Figure 3

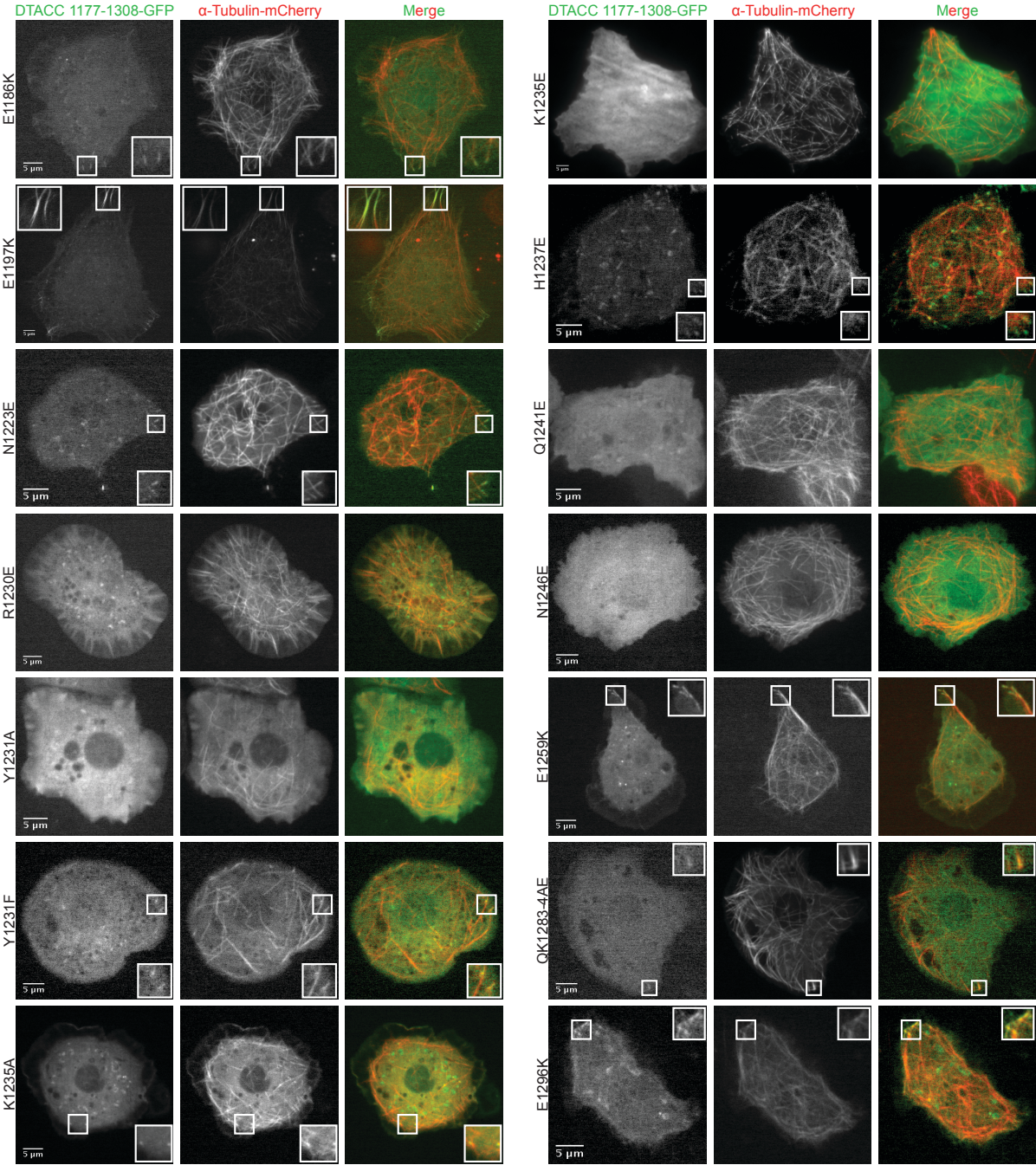


Figure 3. DTACC 1177-1308 mutational analysis during interphase. Endogenous DTACC was knocked down in S2 cells using dsRNA against the N-terminal *dtacc* coding region. Truncated DTACC-GFP constructs (1177-1308) with single charge reversal/ablation mutations were transfected into the cells. An  $\alpha$ -Tubulin-mCherry construct was co-transfected to label MTs, and we observed the mutant DTACC constructs' localization to MT plus-ends during interphase using fluorescence microscopy. The above images are representative cells of each construct's ability to localize to either the MT lattice or MT plus-ends. Quantification of localization ablation for these constructs is in Figure 4.

Figure 4

A

DTACC 1177-1308					
Mutation Construct	n <sub>day</sub>	n <sub>cell</sub>	MT Plus-end (% cells)	MT Lattice (% cells)	Cytoplasmic (% cells)
E1186K	2	18	77.777	83.333	16.6667
E1196K	1	9	66.6667	66.6667	33.3333
N1223E	2	13	92.307	53.846	7.692
R1230E	3	25	0	8	92
Y1231A	2	15	20	0	80
Y1231F	2	22	77.2727	68.1818	18.1818
K1235A	3	15	60	60	22.66667
K1235E	2	16	0	12.5	81.25
H1237E	2	17	76.47059	70.588	17.6471
Q1241E	4	31	22.58065	16.129	51.6129
N1246E	3	17	0	17.64706	58.823
E1259K	3	33	36.36	27.2727	24.2424
QK1283-4AE	2	13	38.4615	46.15385	53.846
E1296K	2	22	68.1818	50	27.27273
Wild Type	2	36	88.888	88.888	11.111

B

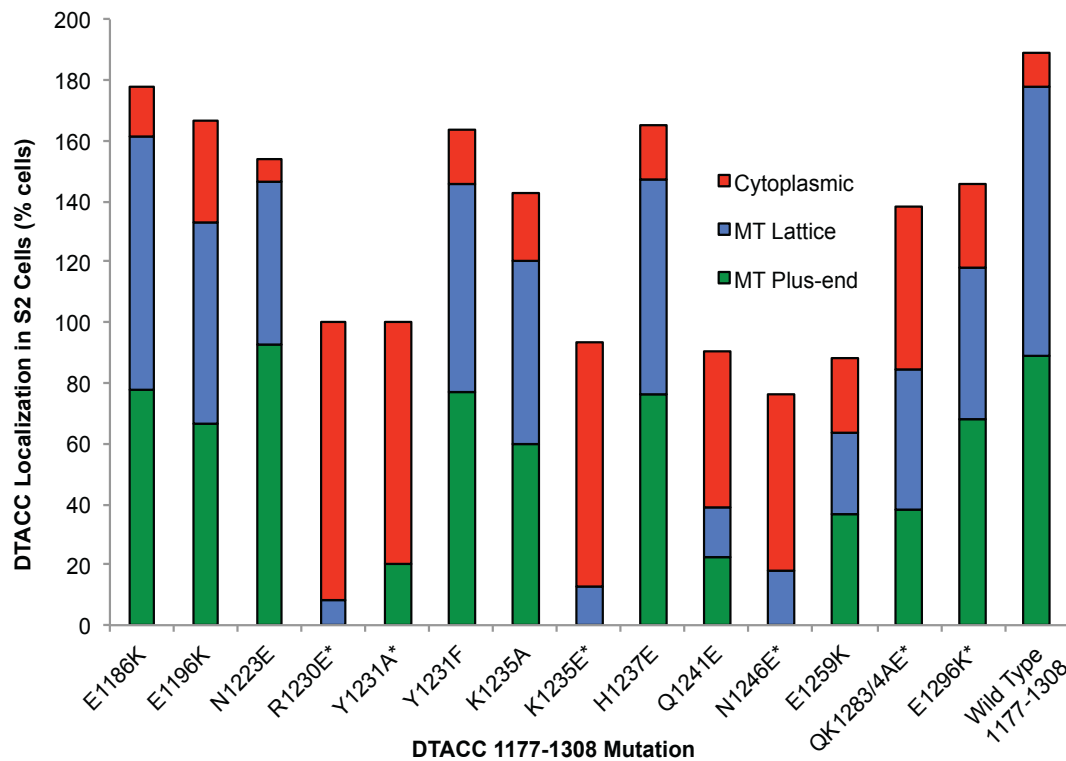
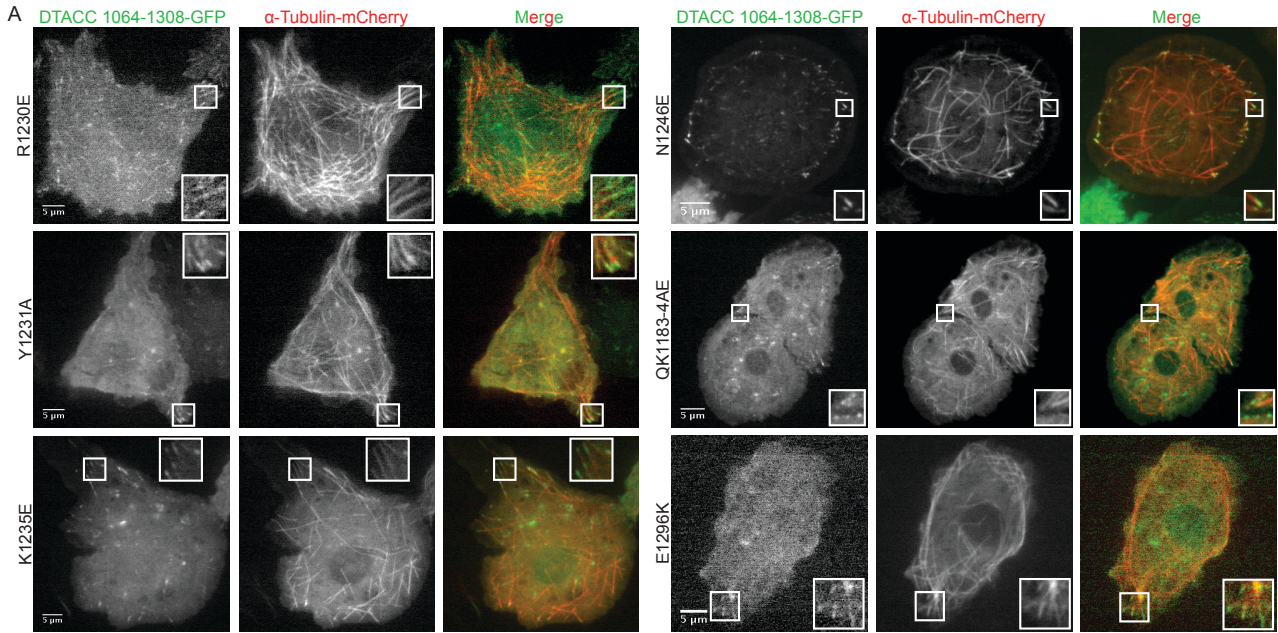


Figure 4. Quantification of DTACC 1177-1308 mutation localization during interphase. (A) This spreadsheet represents the total number of cells for each construct that exhibited localization of mutant DTACC 1177-1308 to MT plus-ends and to the MT lattice. Cells without any noticeable DTACC punctae along MTs were marked “cytoplasmic.” WT DTACC 1177-1308 is presented in the bottom row for comparison. (B) Graphical representation of data presented in (A). Mutations marked with \* were selected for further analysis in DTACC 1064-1308 (Figure 5).

Figure 5



B

DTACC 1064-1308					
Mutation Construct	n <sub>day</sub>	n <sub>cell</sub>	MT Plus-end (% cells)	MT Lattice (% cells)	Cytoplasmic (% cells)
R1230E	2	15	100	100	0
Y1231A	2	15	100	100	0
K1235E	1	7	100	85.714	0
N1246E	1	9	100	77.778	0
QK1283-4AE	1	8	100	100	0
E1296K	2	8	100	75	0
Wild Type	3	27	96.296	96.296	3.703

C

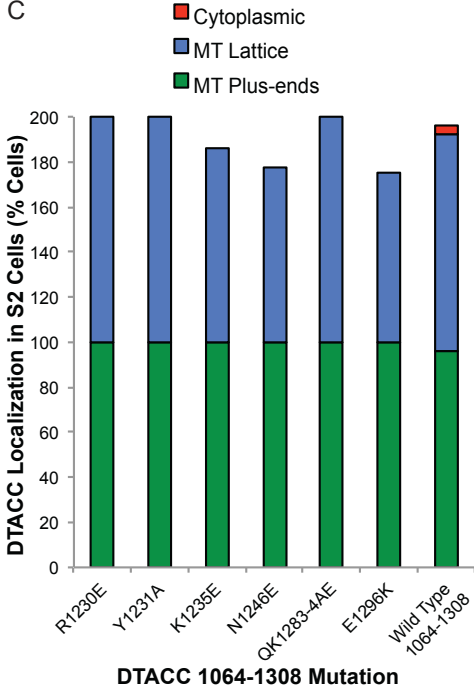
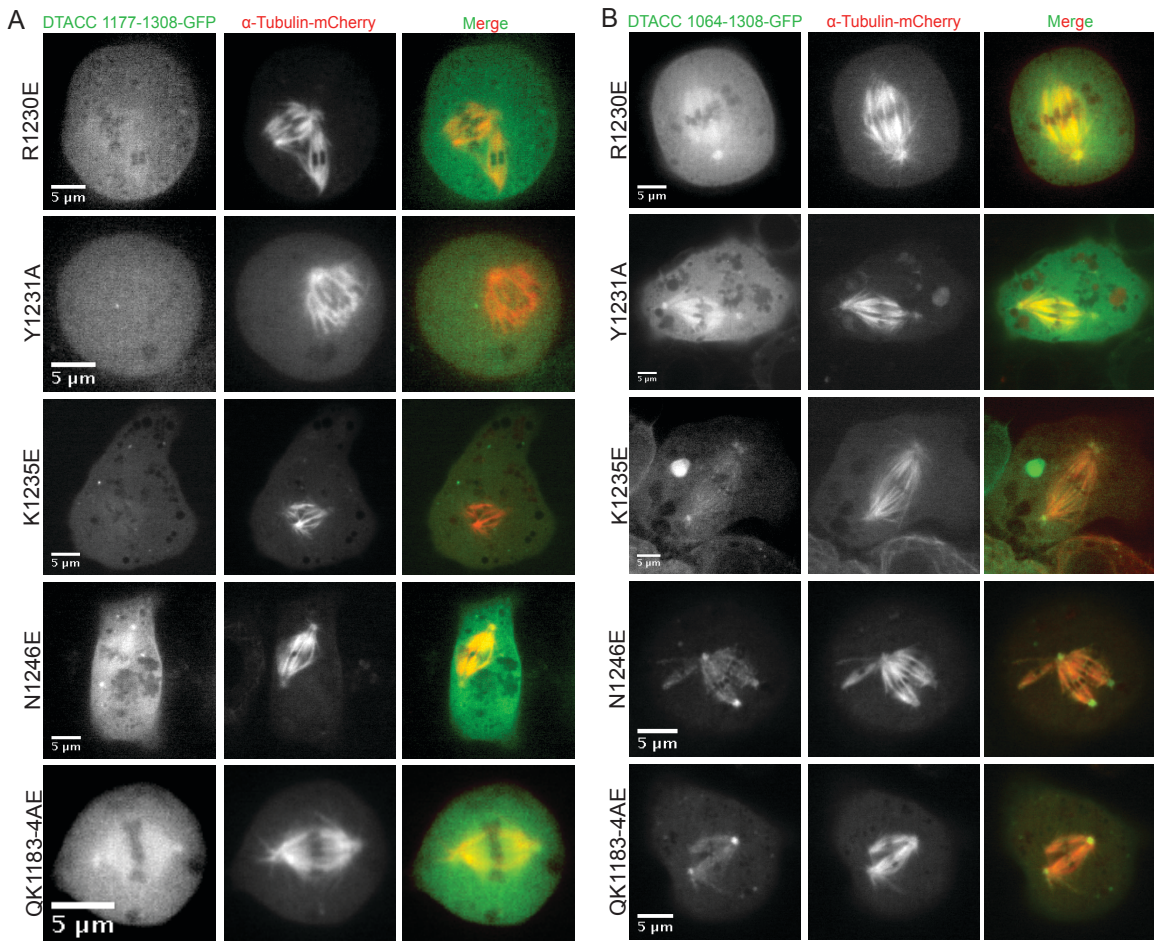


Figure 5. DTACC 1064-1308 mutational analysis during interphase. A subset of the mutations made to 1177-1308 were selected for study in the full DTACC TACC domain using S2 cells and fluorescence microscopy. Representative images of the MT localization ability of each 1064-1308 mutant DTACC construct are shown in (A). Every construct was observed to localize robustly to MT plus-ends. (B) Spreadsheet showing the data for all imaged cells with mutant DTACC 1064-1308. (C) Graphical representation of data presented in (B). Wild type 1064-1308 localization patterns are presented for comparison.

Figure 6



C

Mutation Construct	DTACC 1177-1308			DTACC 1064-1308		
	$n_{\text{day}}$	$n_{\text{cell}}$	Centrosome Localization (% cells)	$n_{\text{day}}$	$n_{\text{cell}}$	Centrosome Localization (% cells)
R1230E	2	6	18.18181	2	4	100
Y1231A	2	9	0	1	3	100
K1235E	2	3	33.3333	1	2	100
N1246E	3	7	100	1	3	100
QK1183-4AE	2	5	80	1	3	100

D

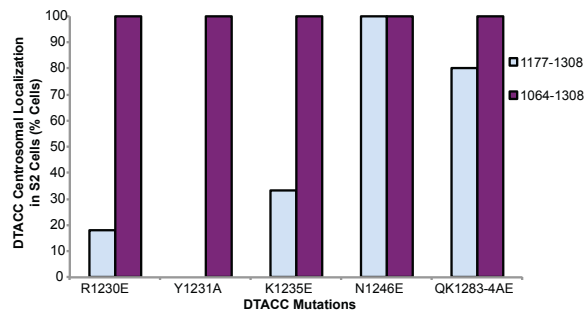


Figure 6. DTACC mutational analysis during mitosis. (A) Mitotic S2 cells transfected with the same mutant DTACC as in Figures 3-5. Representative images of each mutant construct in both 1177-1308 (A) and 1064-1308 (B). We observed and quantified (C) the ability of each mutant construct to localize to centrosomes during mitosis. (D) Graphical representation of data presented in (C). Most DTACC 1064-1308 mutants showed more robust localization to centrosomes than did the corresponding mutants in 1177-1308.

(representative interphase images in Figure 5A). The cells for each 1064-1308 mutation were scored according to the same guidelines as in 1177-1308, the data for which is in Table 5B. The accompanying graph (Figure 5C) visually presents this MT localization data for each 1064-1308 mutation in comparison to WT DTACC 1064-1308.

Mitotic cells for each mutant construct (in both 1177-1308 and 1064-1308) were also scored on the ability for their mutant DTACC to localize to centrosomes. Mitotic cells were rare to find while imaging, so the five pairs of mutant constructs in Figure 6 represent those constructs with enough mitotic cells to quantify (Table 6B) and clearly present (Figure 6C) their mutant DTACC centrosomal localization patterns. Figure 6C shows a comparison of the effects of each mutation on centrosome localization when it is directed to DTACC 1177-1308 and to DTACC 1064-1308.

### C. DTACC and Msps Interact Directly in Cells and *in vitro*

We not only hypothesize that DTACC's interaction with Msps is mediated by its coiled-coil, we also hypothesize that this interaction is direct and that the C-terminal domains of each protein are sufficient for this interaction. I tested for this direct interaction in cell culture using a KnockSideways system in S2 cells. I first transfected the cells with an exogenous, truncated Msps-GFP c-terminal construct (residues 1596-2042) to observe its localization. Msps 1596-2042-GFP was unremarkably cytoplasmic in these singly transfected cells (Figure 7A). However, when I co-transfected S2 cells with both Msps 1596-2042-GFP and mito-tRFP-DTACC 1064-1308 (genetically designed to be targeted to mitochondria), both Msps-GFP and mito-tRFP-DTACC robustly and consistently co-localized to mitochondrial membranes (Figure 7B).

Figure 7

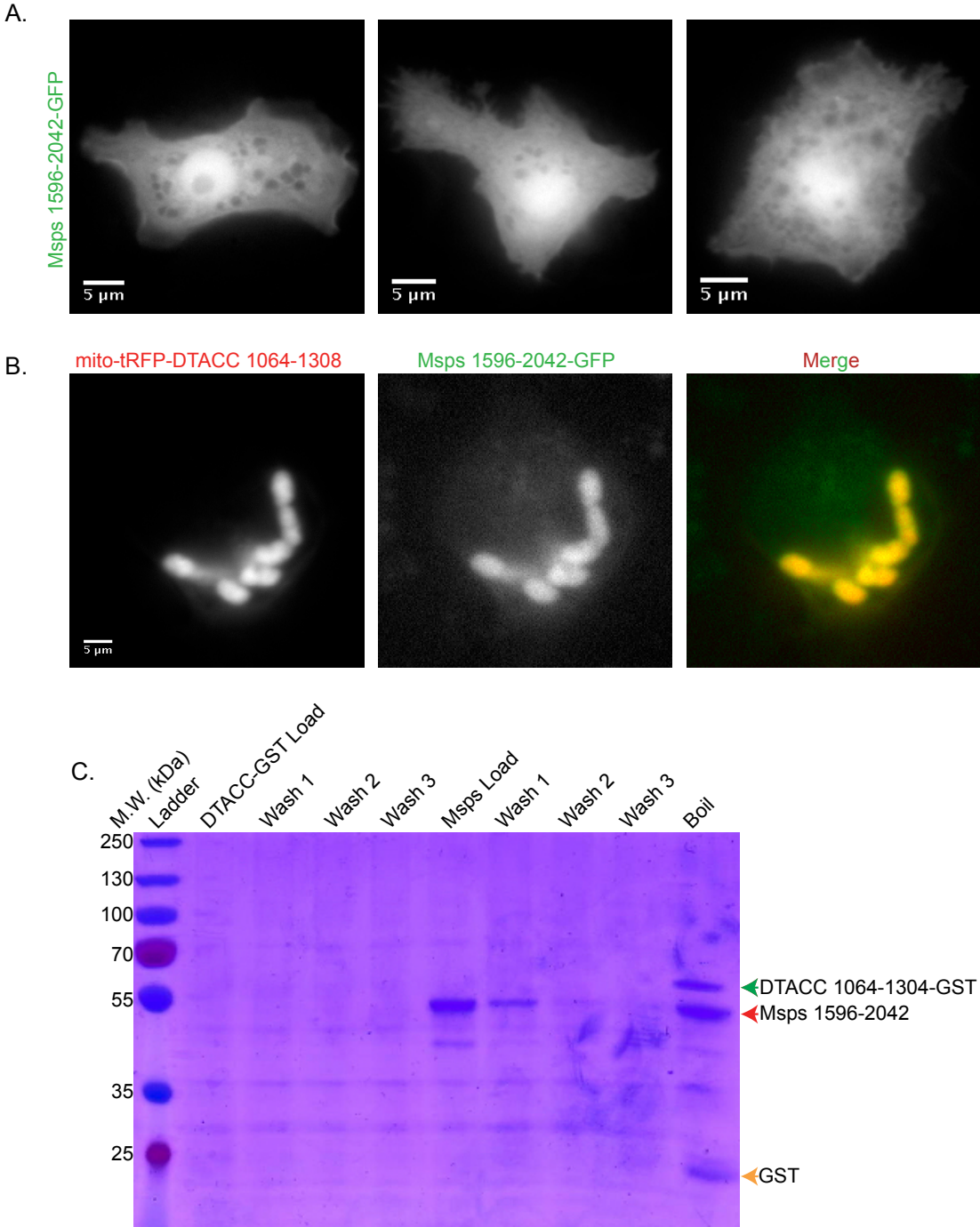


Figure 7. DTACC-Msp1596 interaction. (A) Msp1596-2042-GFP does not localize to mitochondria when transfected into S2 cells alone; (B) Msp1596-2042-GFP is successfully knocked sideways into the mitochondrial membrane when co-transfected with DTACC mito-tRFP-DTACC 1064-1308, suggesting that these two constructs interact in cell culture. (C) DTACC 1064-1304-GST is able to pull down the same Msp1596-2042 construct *in vitro*. The predicted molecular weights of DTACC 1064-1304-GST (green arrow), Msp1596-2042 (red arrow), and GST (orange arrow) are 53.8 kDa, 50.4 kDa, and 28 kDa, respectively.

To test the same DTACC-Msps interaction *in vitro*, I used a GST pull-down assay in which I tested the ability of purified DTACC 1064-1304-GST to bind purified Msps 1596-2042 (Figure 7C). DTACC 1064-1308-GST was first conjugated to glutathione beads alone (DTACC-GST Load, Figure 7C). After addition of Msps 1596-2042 (Msps Load, Figure 7C), three washes removed any unbound Msps, as can be seen by the Wash 1-3 lanes (Figure 7C). After denaturation of the beads by SDS and boiling, the DTACC-GST was unbound from the beads and separated by SDS-PAGE (Boil, Figure 7C). DTACC 1064-1304-GST (M.W. = 53.8 kDa, green arrow, Figure 7C) and Msps 1596-2042 (M.W. = 50.4 kDa, red arrow, Figure 7C) protein bands are present in the boil lane, indicating that the Msps C-terminal domain (CTD) bound directly to the bead-conjugated DTACC 1064-1304-GST.

## Discussion

The concept that structure determines function is one of the most fundamental principles in all levels of biology. This principle strongly applies to protein-protein interactions; it is not possible to fully understand the role a protein plays in a cell or how it interacts with other proteins without elucidating the structural basis of these functions. The MT cytoskeleton is no exception to this principle; its structure is constantly undergoing rearrangements as MTs dynamically cycle between phases of growth, pause, and shrinkage. It is this dynamicity that affords MTs their functional versatility. Without the ability to reorganize, the MT lattice would cease to perform its most essential functions of cell motility, intracellular transport, and chromosome segregation.

Because MAPs contribute to the regulation of the MT lattice in cells, understanding the mechanisms by which they regulate MTs is central to the understanding of how MTs carry out

their diverse and vitally important roles. The TACC family of MAPs is known to be essential for proper MT spindle formation during mitosis (Raff *et al.*, 2002), but the specific mechanism by which it executes this function is still poorly understood. Its association with the well-studied XMAP215 MT polymerase family has provided clues as to how it confers stability to the mitotic spindle, but there is still little to no structural information on most of the TACC family, nor a definitive structural mechanism for its interaction with XMAP215.

Characterizing the TACC domain function using structural methods was based on the hypothesis that the DTACC TACC domain is a coiled-coil. The TACC domain in DTACC is the only part of the protein that is sufficient to confer localization to MTs (Figure S2), and secondary structure predictions indicate a high probability of coiled-coil formation in this domain. Coiled-coils are formed by alpha helices, so I tested the alpha helical character of different truncations of the TACC domain using CD (Figure 1). All three truncations (1064-1176, 1177-1304, and 1064-1304) all showed strong alpha helical character with CD minima at 208 and 222 nm (Figure 1A,C,E). This supports the TACC domain coiled-coil hypothesis. However, the temperature ramp CDs of each truncation construct revealed that neither 1177-1304 or 1064-1176 (Figure 1B,D) are as thermally stable as the full TACC domain (Figure 1F), this supports the hypothesis that the entire TACC domain is responsible for *stable* coiled-coil formation.

Coiled-coil domains often confer homodimerization, so we also tested the tendencies of the same three TACC domain truncations to homodimerize using SEC-MALS (Figure S4). Both 1064-1304 and 1177-1304 dimerized *in vitro* (Figure S4 A,C), whereas 1064-1176 remained a monomer (Figure S4 B). In combination with the CD results, the SEC-MALS data suggest that DTACC 1064-1304 forms a stable coiled coil dimer and that DTACC 1177-1304 forms a less stable coiled coil dimer. These results suggest that DTACC 1064-1176 is not sufficient to form a

coiled coil by itself, but instead that these residues afford extra stability to the overall structure of the entire TACC domain. Our structural characterizations of the *Drosophila* TACC coiled-coil domain are consistent with recently published crystal structures TACC family members in other species, including XTACC3 in *Xenopus* (Mortuza *et al.*, 2014) and TACC3 in humans (Guo *et al.* 2015). This consistency in alpha helicity and dimerization in various homologues suggests that the TACC domain coiled-coil structure, as well as its sequence, is conserved throughout evolution.

The structural insights provided by the CD and SEC-MALS can be applied to DTACC's localization patterns in S2 cells. Our lab has previously shown that both DTACC 1064-1304 and 1177-1304 are sufficient to localize to MT plus-ends and to centrosomes, whereas DTACC 1064-1176 is not sufficient (Figure S2). These localization trends mirror the dimerization trends for each respective DTACC construct, suggesting a link between DTACC's ability to form dimeric coiled-coils and its ability to localize to MTs and centrosomes. In addition, our lab has also previously shown that DTACC's localization to MTs is mediated by the presence of Msps (Figure S1). Therefore, the CD and SEC-MALS results suggest that DTACC interacts with Msps via a coiled-coil in its C-terminal TACC domain.

The hypothesis that DTACC forms and interacts with Msps through a coiled-coil domain is also central to the *in vivo* mutational analysis in Figures 3-6. If DTACC does form a coiled-coil dimer, then certain hydrophobic residues in the C-terminal alpha helices should be involved in forming the DTACC dimerization interface, while other solvent-exposed residues should be involved in forming the DTACC-Msps binding interface. The TACC family sequence identity/homology alignment was used to identify conserved, charged residues (Figure S3, red boxes). We thus predict that the charged side chains of these residues formed the solvent-

exposed surface of the putative coiled coil, and we tested this through individually ablating or reversing these charges through mutation and observing the mutant DTACC's localization patterns during interphase (Figures 3-5).

Theoretically, mutating a charge reversal or ablation in DTACC's putative coiled-coil should not disrupt the formation of the coiled-coil, but should merely alter the distribution of charge along the coiled-coil surface. Thus, if Msps binds DTACC's putative coiled-coil through a charge-specific mechanism, and an essential DTACC surface charge is reversed, Msps binding to DTACC should weaken. If the DTACC-Msps binding is weakened, it should be evident in the particular mutant construct's localization to MT plus ends.

Not all mutations made to DTACC 1177-1308 had equal effects on DTACC's ability to localize to MT plus-ends (tip-track), as is shown in Figure 4B. Specifically, mutations made in the region 1230-1246 severely ablated DTACC's tip-tracking and lattice-binding abilities (R1230E, Y1231A, K1235E, Q1241E, N1246E). Interestingly, it seems that a tyrosine to alanine mutation (charge ablation and size reduction) at residue 1231 has a more deleterious effect on tip-tracking than does a tyrosine to phenylalanine mutation (only charge ablation) at the same residue. This suggests that a specific charge distribution along the putative coiled-coil's surface may not be the only factor conferring Msps binding. In addition, at residue 1235, a lysine to glutamic acid (charge reversal) mutation is more deleterious to tip-tracking than a lysine to an alanine (charge ablation and size reduction). This could suggest that electrostatic interactions play a more important role in Msps binding than size of the residue or presence of charge.

We next selected a subset of the mutations made to 1177-1308 to test further by introducing them into DTACC 1064-1308, the full TACC domain (Figure 5). The same mutations that strongly ablated tip-tracking when present in 1177-1308 (R1230E, Y1231A,

K1235E, N1246E; Figure 4B) all showed robust tip-tracking when present in the full TACC domain (Figure 5C). The localization patterns of the mutants were, in fact, very similar to that of the WT 1064-1308 construct. These stark differences in localization patterns of the same mutations when present in two different DTACC constructs suggests that the additional residues in the full TACC domain (residues 1064-1176) are sufficient to allow even a mutated DTACC construct to tip-track when the TACC domain is not truncated. This observation mirrors the structural observations from the SEC-MALS; namely, that residues 1064-1176 are not sufficient to dimerize or tip-track alone, but still confer greater stability and function to the full TACC domain. This suggests a structural link between DTACC's dimerization and its interaction with Msps. In addition, the results from our mutational analysis of mitotic cells (Figure 6) in both DTACC 1177-1308 and 1064-1308 agree with the interphase analysis. Figure 6D suggests that mutations that ablate DTACC centrosomal localization in 1177-1308 (R1230E, Y1231A, K1235E) do not ablate centrosomal localization when present in DTACC 1064-1308.

Despite the high conservation of TACC and XMAP215 throughout species, the current literature on the TACC family does not agree on the regions of TACC residues that interact with XMAP215 (Hood *et al.*, 2013; Thakur *et al.*, 2014; Mortuza *et al.*, 2014). In a similar fashion, the Msps-interacting region in the *Drosophila* TACC homologue that our mutational analysis identified (residues 1230-1246) does not agree with XMAP215-interacting regions in human TACC3 (Hood *et al.*, 2013; Thakur *et al.*, 2014), *X. laevis* XTACC3 (Mortuza *et al.*, 2014), or *C. elegans* TAC-1 (Bellanger *et al.* 2007). Our results further suggest that while the interaction of the TACC and XMAP215 families is conserved throughout evolution, the specific location of the interaction is significantly different between species.

Despite providing key insights into the putative coiled-coil structure of the TACC domain, our mutational analysis experiments do not illustrate any direct interaction between DTACC and Msps. To examine more direct interactions between the two MAPs, I have begun to develop a combination of cell culture and biochemical techniques to more directly assay the DTACC-Msps interaction. The DTACC-Msps KnockSideways experiment (Figure 7A,B) shows that mito-DTACC 1064-1308 construct can pull Msps 1596-2042 (the C-terminal domain) to mitochondria. The main limitation of this assay is that it is in cell culture, and cannot show definitively that these DTACC and Msps constructs are directly binding to each other, rather than through some intermediate or in a larger complex.

To supplement this KnockSideways experiment, I have used GST pull downs with the same Msps and DTACC constructs as in cell culture to show that the two purified constructs can directly bind *in vitro* (Figure 7C). While I have not yet purified or cloned the various DTACC and Msps constructs necessary to test more specific combinations of DTACC/Msps constructs, this KnockSideways/Pull Down system will be eventually combined with my DTACC mutational constructs to more directly assay for ablation of Msps binding. This *in vitro*/cell culture system will be more accurate at determining the competence of the direct DTACC-Msps interaction than the indirect method of analyzing DTACC's tip-tracking abilities in cell culture alone.

Ultimately, the insights into the TACC domain gained by the combination of CD, SEC-MALS, and mutational analysis are not definitive structural characterizations. These biochemical and cell biological results would be invaluable supplements to a crystal structure of the TACC domain. Figure 2 shows my preliminary attempts to crystallize DTACC 1064-1304 using commercial broad-screen and optimization techniques. The crystals that have grown are

irregularly shaped and likely unsuitable for X-ray crystallography. More optimization is needed to obtain more uniform and repeatable crystals, both in the protein purification and crystallization processes. The lack of structure in all but the most recent literature attests to the difficulty of any definitive structural characterization of TACC family members, as the only results have been produced by low-resolution small-angle X-ray scattering (SAXS) (Mortuza *et al.*, 2014) or by complexing TACC proteins to unnatural binding partners to confer crystallization (Guo *et al.*, 2015).

The overall lack of structural information on DTACC and the DTACC-Msps interaction prevents us from definitively understanding how DTACC functions as a centrosomal regulator of MTs during mitosis. The truncational and mutational experiments to the DTACC TACC domain have provided support for the coiled-coil structure of the DTACC TACC domain, as well as its putative role in mediating Msps binding through conserved charged residues. These experiments will ultimately contribute to our understanding of the interactions of the entire TACC and XMAP215 protein families, and how they participate in the fidelity of the mitotic bipolar spindle reorganization and stabilization.

### **Acknowledgements**

I would like to thank my thesis advisor, Dr. Kevin Slep, as well as my two graduate student mentors, Dr. Jaime Fox and Rebecca Adikes, for their guidance during this research project and throughout my undergraduate career. I would also like to thank Dr. Ashutosh Tripathy at UNC MAC-IN-FAC for his assistance with CD, and Dr. Steve Rogers for cloning constructs.

## Literature Cited

- Albee, A.J. and Wiese, C. (2008) *Xenopus* TACC3/Maskin Is Not Required for Microtubule Stability but Is Required for Anchoring Microtubules at the Centrosome. *MBOC* **19**, 3347-3356.
- Booth, D.G, Hood, F.E., Prior, I.A., and Royle, S.J. (2011) A TACC3/ch-TOG/clathrin complex stabilises kinetochore fibres by inter-microtubule bridging. *EMBO J.* **30**, 906-919.
- Bellanger, J.M., and Gönczy, P. (2003) TAC-1 and ZYG-9 Form a Complex that Promotes Microtubule Assembly in *C. elegans* Embryos. *Curr. Bio.* **13**, 1488-1498.
- Bellanger, J.M., Carter, J.C., Phillips, J.B., Canard, C., Bowerman, B., and Gönczy, P. (2007) ZYG-9, TAC-1 and ZYG-8 together ensure correct microtubule function throughout the cell cycle of *C. elegans* embryos. *J. Cell Sci.* **120** (16) 2963-2973.
- Gergely, F., Karlsson, K., Still, I., Cowell, J., Kilmartin, J., and Raff, J.W. (2000) The TACC domain identifies a family of centrosomal proteins that can interact with microtubules. *PNAS* **97**, 14352-57.
- Glover, D.M., Gonzales, C., and Raff, J.W. (1993) The Centrosome. *Sci. Am.* **268**, 62-68.
- Guo, Y., Scheuermann, T.H., Partch, C.L., Tomchick, D.R., and Gardner, K.H. (2015) Coiled coil Coactivators Play a Structural Role Mediating Interactions in Hypoxia Inducible Factor Heterodimerization. *JBC*, M114.632786.
- Hood, F.E., Williams, S.J., Burgess, S.G., Richards, M.W., Roth, D., Straube, A., Pfuhl, M., Bayliss, and Royle, S.J. (2013) Coordination of adjacent domains mediates TACC3-ch-TOG-clathrin assembly and mitotic spindle binding. *JCB* **202** (3), 463-78.
- Mortuza, G.B., Cavazza, T., Garcia-Mayoral, M.F., Hermida, D., Peset, I., Pedrero, J., Merino, N., Blanco, F.J., Lyngsø, J., Bruix, M. Pedersen, J.S., Vernos, I., and Montoya, G. (2014) XTACC3-XMAP215 association reveals an asymmetric interaction promoting microtubule elongation. *Nat. Comm.* **5**.
- Peset, I., and Vernos, I. (2008) The TACC Proteins: TACC-ling Microtubule Dynamics and Centrosome Function. *Trends In Cell Bio.* **18** (8), 379-88.
- Raff, J.W. (2002) Centrosomes and Cancer: Lessons from a TACC. *Trends In Cell Bio.* **12** (5), 222-25.
- Still, I.H., Vince, P., and Cowell, J.K. (1999) The third member of the transforming acidic coiled coil containing gene family, TACC3, maps in 4p16, close to translocation breakpoints in multiple myeloma, and is upregulated in various cancer cell lines. *Genomics* **58**, 165-170.
- Shirasu-Hiza, M., Coughlin, P., and Mitchinson, T. (2003) Identification of XMAP215 as a microtubule-destabilizing factor in *Xenopus* egg extract by biochemical purification. *JCB* **161** (2), 349-58.
- Thakur, H.C., Singh, M., Nagel-Steger, L., Kremer, J., Prumbaum, D., Fansa, E.K., Ezzahoni, H., Nouri, K., Gremer, L., Abts, A., Schmitt, L., Raunser, S., Ahmadian, M.R., and Piekorz, R.P. (2013) The Centrosomal Adaptor TACC3 and the Microtubule Polymerase chTOG Interact via Defined C-terminal Subdomains in an Aurora-A Kinase-independent Manner. *JBC* **289**, 74-88.
- Tuszynski, J.A., Trpišová, B., Sept, D., and Brown, J.A. (1997) Selected Physical Issues in the Structure and Function of Microtubules. *Journ. of Str. Bio.* **118**, 94-106.

Supplementary Figures

Figure S1

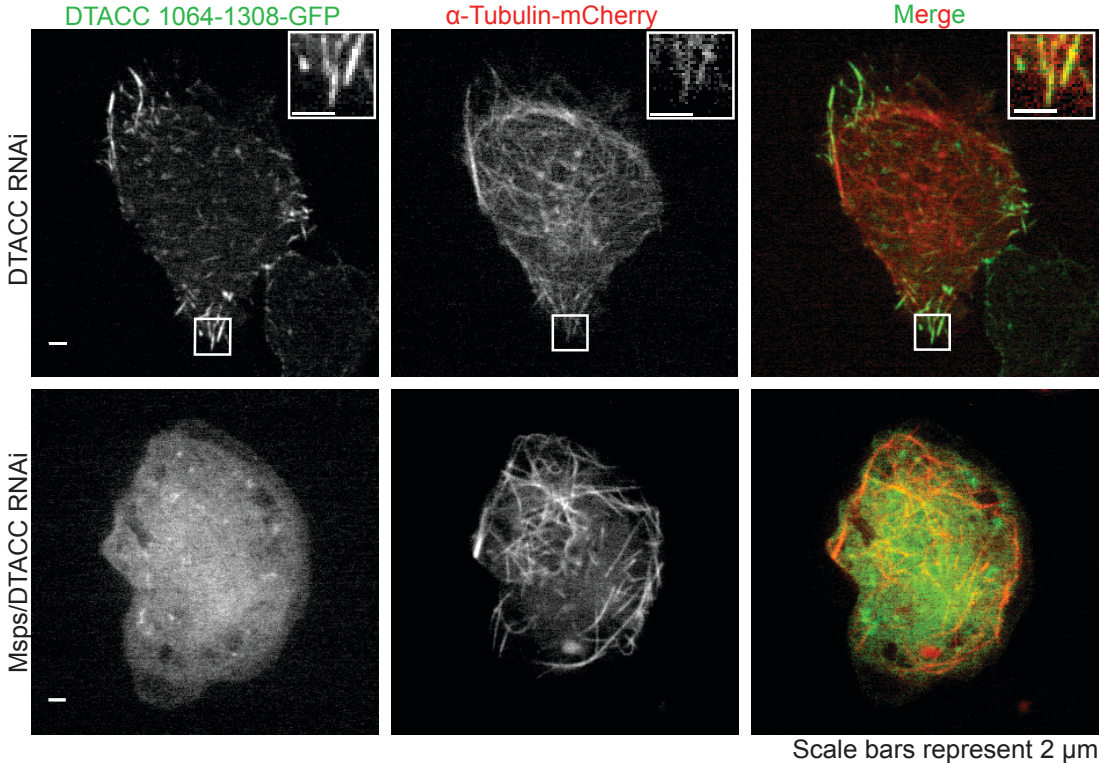


Figure S1: DTACC/Msp double knockdown. Transfection of exogenous DTACC 1064-1308 in an RNAi-depleted endogenous DTACC background shows localization to MTs. However, if endogenous DTACC and Msp are co-depleted by RNAi (bottom row), exogenous DTACC 1064-1308-GFP can no longer localize to MTs. These data suggest that Msp is necessary for TACC domain MT plus-end localization. We thus use DTACC's localization to MT plus-ends during interphase as a read-out for DTACC's interaction with Msp in cell culture.

Figure S2

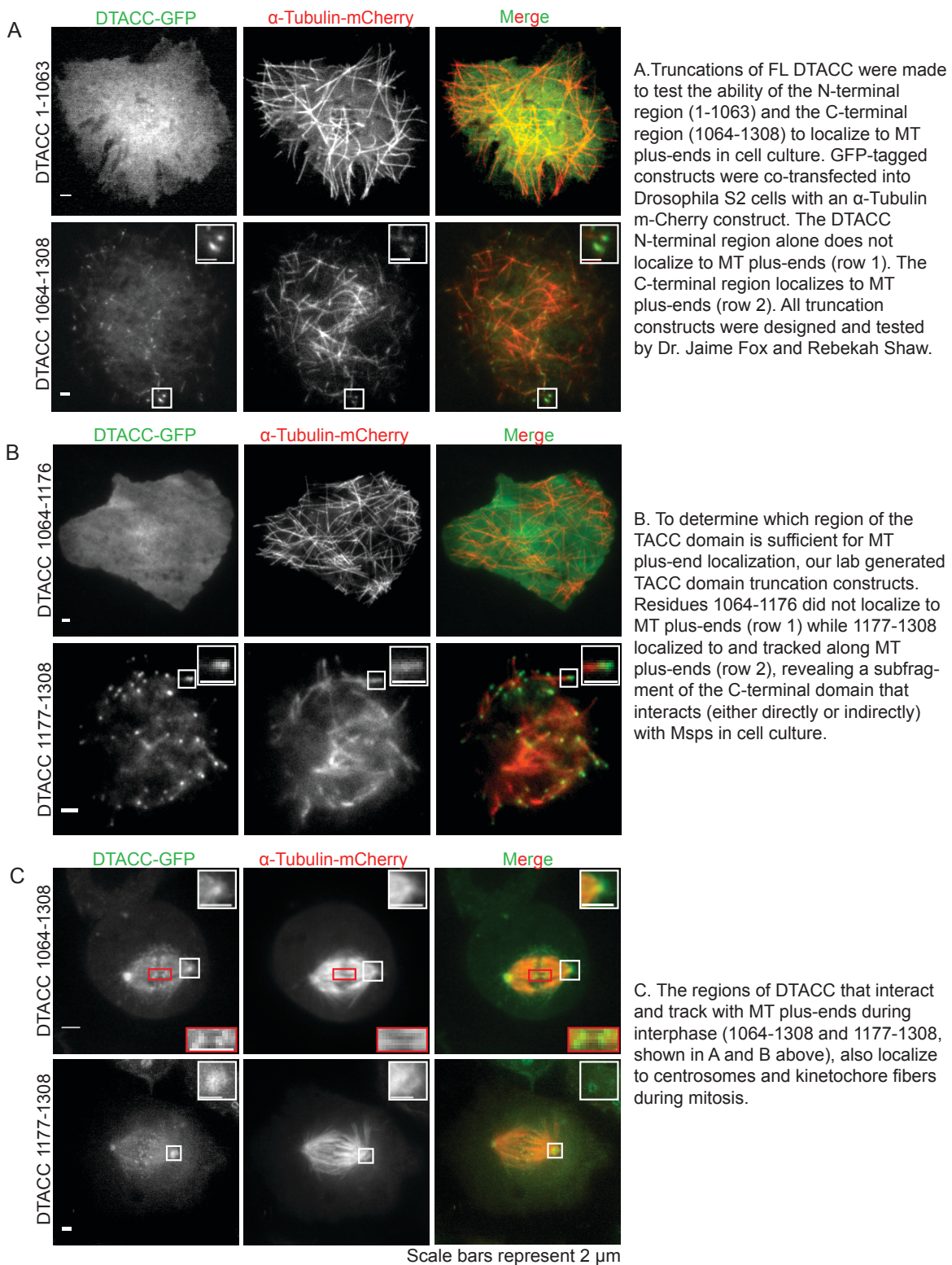


Figure S3

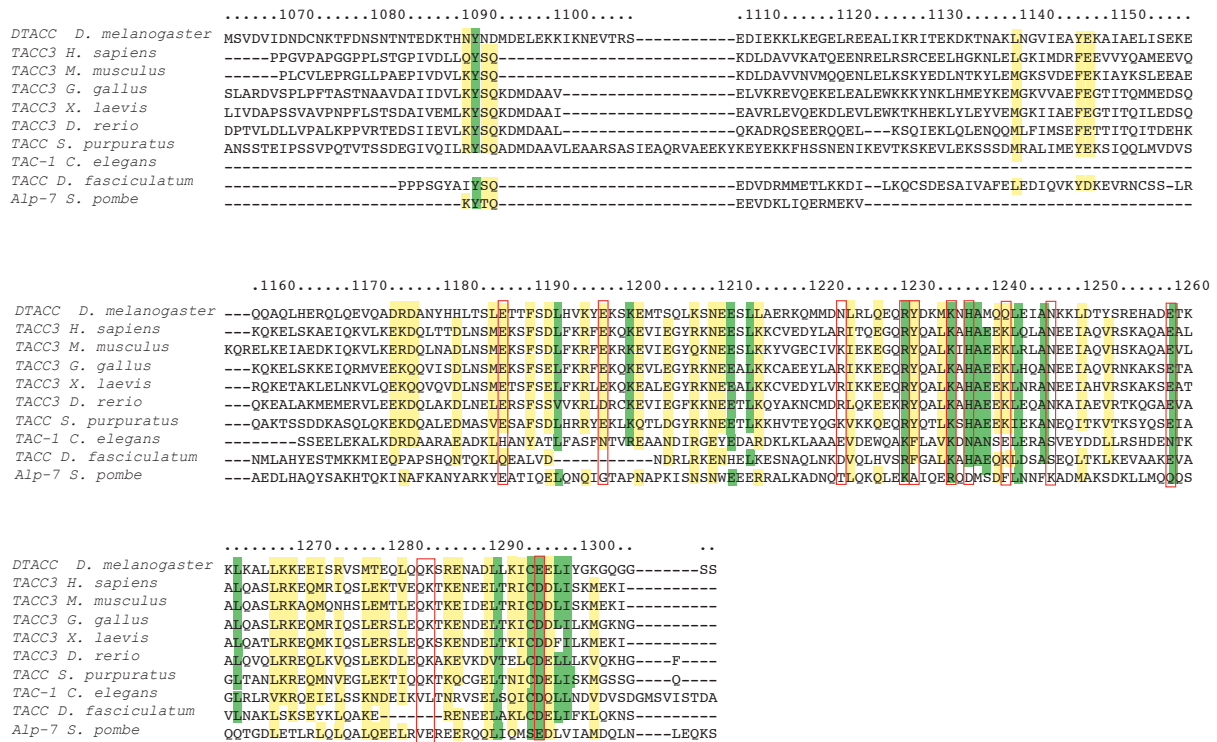
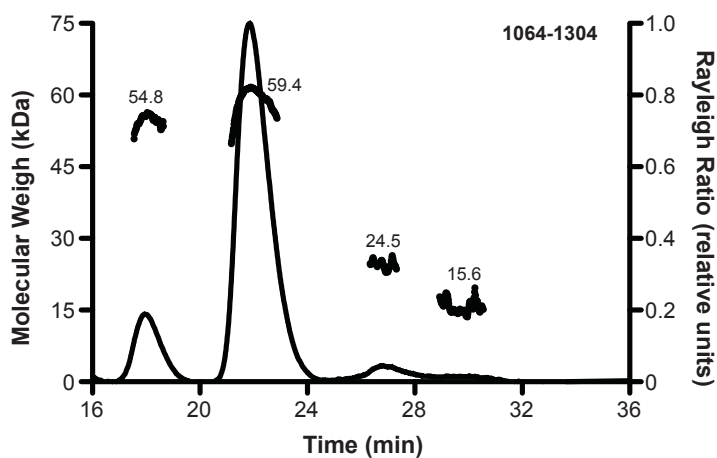


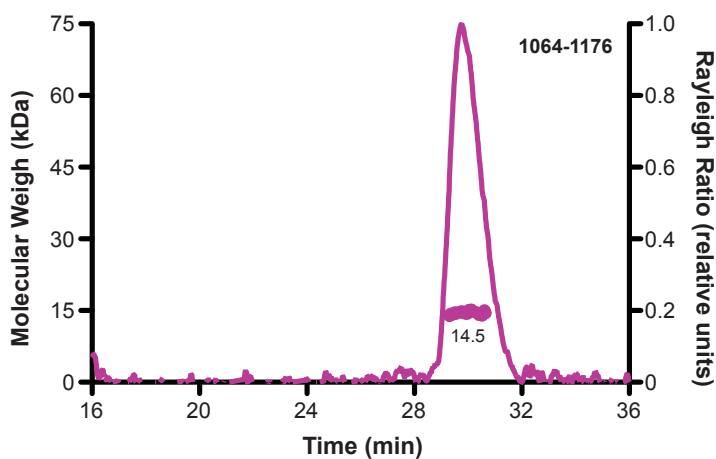
Figure S3. Sequence alignment between DTACC and evolutionary homologues. Green = 80% identity, yellow = 80% homology. Red boxes indicate DTACC residues tested using mutational analysis. Residues were chosen based on charge conservation.

Figure S4

A.



B.



C.

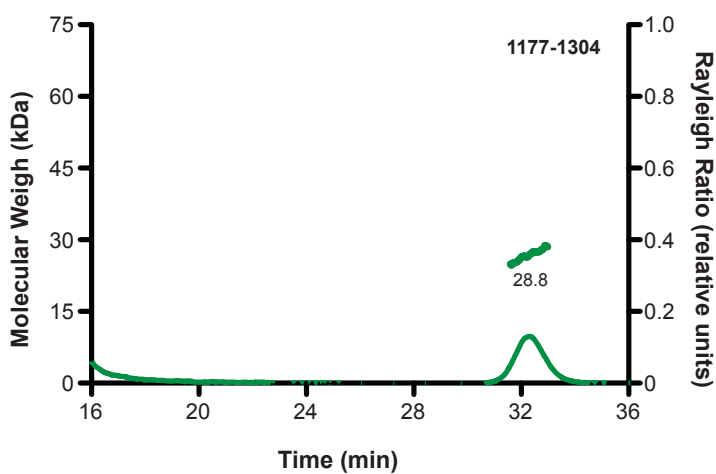


Figure S4. SEC-MALS for DTACC TACC domain truncations. SEC-MALS was performed on the full TACC domain (A), and its two truncations, 1064-1176 (B) and 1177-1308 (C). Dynamic light scattering in (A) shows DTACC 1064-1304 exists as a dimer population at a M.W. of 59.4 (predicted monomer M.W. = 28.3). Similarly, (C) shows DTACC 1177-1308 dimerizes *in vitro* (predicted monomer M.W. = 15.2). However, 1064-1176 exists as a monomer in (B) (predicted monomer M.W. = 13.1 kDa). All protein purification and SEC-MALS was performed by Rebecca Adikes.